An upper tropospheric humidity data set from operational satellite microwave data

S. A. Buehler,[1] M. Kuvatov,[2,5] V. O. John,[3,6] M. Milz,[1] B. J. Soden,[3] D. L. Jackson,[4] and J. Notholt[2]

[1]   183.31 GHz observations from the Advanced Microwave Sounding Unit B (AMSU-B) instruments onboard the NOAA 15, 16, and 17 satellites were used to derive a new data set of Upper Tropospheric Humidity (UTH). The data set consist of monthly median and mean data on a 1.5° latitude-longitude grid between 60°S and 60°N, and covers the time period of January 2000 to February 2007. The data from all three instruments are very consistent, with relative difference biases of less than 4% and relative difference standard deviations of 7%. Radiometric contributions by high ice clouds and by the Earth's surface affect the measurements in certain areas. The uncertainty due to clouds is estimated to be up to approximately 10%RH in areas with deep convection. The uncertainty associated with contamination from surface emission can exceed 10%RH in midlatitude winter, where the data therefore should be regarded with caution. Otherwise the surface influence appears negligible. The paper also discusses the UTH median climatology and seasonal cycle, which are found to be broadly consistent with UTH climatologies from other sensors. Finally, the paper presents an initial validation of the new data set against IR satellite data and radiosonde data. The observed biases of up to 9%RH (wet bias relative to HIRS) were found to be broadly consistent with expectations based on earlier studies. The observed standard deviations against all other data sets were below 6%RH. The UTH data are available to the scientific community on http://www.sat.ltu.se.

1.   Introduction

[2]   Water vapor in the upper troposphere is responsible for a large part of the atmospheric greenhouse effect. Furthermore, the feedback associated with this parameter significantly amplifies the response of the climate system to changes in anthropogenic greenhouse gases such as carbon dioxide [*Held and Soden*, 2000]. The amount of total water vapor in the atmosphere is expected to increase as the climate warms [*Trenberth et al.*, 2005], but the changes in upper tropospheric water vapor in a warming climate have been the subject of debate [e.g., *Lindzen et al.*, 2001; *Minschwaner and Dessler*, 2004; *Soden et al.*, 2005]. Recent modeling studies indicate that climate models all show similar water vapor feedback broadly consistent with that expected from a constant relative humidity increase in upper tropospheric water vapor, despite the fact that they have very different humidity mean states [*John and Soden*, 2007; *Soden and Held*, 2006]. However, the available data for upper tropospheric water vapor are neither sufficient to quantify long-term changes, nor sufficient to evaluate climate models [*de F. Forster and Collins*, 2004].

[3]   The longest available humidity data record is from radiosondes. However, radiosonde humidity measurements can suffer from significant biases [*Elliott et al.*, 2002; *Soden and Lanzante*, 1996] which make it hard to use that data record for climate monitoring. Even comparatively high quality radiosonde data contain significant biases [*Soden et al.*, 2004; *Buehler et al.*, 2004]. Another drawback is that the spatial coverage of radiosonde measurements is poor.

[4]   Due to their global coverage, satellite measurements have a great potential for climate studies. Several research satellite instruments measure upper tropospheric water vapor, for example the Microwave Limb Sounder (MLS) [*Read et al.*, 1995; *Cuddy et al.*, 2006] and the Atmospheric Infrared Sounder (AIRS) [*Aumann et al.*, 2003]. Several

[1]Institutionen för Rymdvetenskap (Department of Space Science) (IRV), Luleå University of Technology, Kiruna, Sweden.
[2]Institut für Umweltphysik (Institute for Environmental Physics) (IUP), University of Bremen, Bremen, Germany.
[3]Meteorology and Physical Oceanography, Rosenstiel School for Marine and Atmospheric Science (RSMAS), University of Miami, Miami, Florida, USA.
[4]Cooperative Institute for Research in Environmental Science (CIRES), University of Colorado/NOAA Earth System Research Laboratory, Boulder, Colorado, USA.
[5]Now at German Weather Service (Deutscher Wetterdienst, DWD), Offenbach am Main, Germany.
[6]Now at Met Office Hadley Centre, FitzRoy Road, Exeter, UK.

Table 1. Channel Characteristics of the AMSU-B Instrument From the NOAA KLM User Guide (http://www2.ncdc.noaa.gov/docs/klm/)

Channel	Center Freq., GHz	NEΔT, K
16	89.0 ± 0.9	0.37
17	150.0 ± 0.9	0.84
18	183.31 ± 1.0	1.06
19	183.31 ± 3.0	0.7
20	183.31 ± 7.0	0.6

studies were carried out using these data sets. For example, *Gettelman et al.* [2006] found that upper tropospheric humidity calculated from AIRS observations shows variability on multiple timescales, ranging from seasonal variations to high frequency variations associated with baroclinic storms.

[5] Unfortunately, data from these instruments are only available for relatively short time periods, which limits their use for creating a long-term data record. In contrast to this, instruments on operational meteorological satellites provide consistent and long-term measurements. In general, two frequency regions are used to measure water vapor operationally, one in the infrared (IR) spectral region near 6.3 μm and another one in the microwave spectral region near 183.31 GHz. The IR measurements are available from geostationary and polar orbiting satellites, whereas the microwave measurements are only available from polar orbiting satellites.

[6] The IR instrument HIRS [*Smith et al.*, 1979] provides the longest available upper tropospheric humidity (UTH) record from satellite measurements, dating back to 1979. UTH is defined here as the Jacobian-weighted relative humidity in the upper troposphere (see *Soden and Bretherton* [1996] for details). Numerous scientific studies have been conducted using these data [e.g., *Soden and Bretherton*, 1996; *Spangenberg et al.*, 1997; *Bates and Jackson*, 2001; *Bates et al.*, 2001; *Allan et al.*, 2003; *Soden et al.*, 2005].

[7] A shortcoming of IR data in general is that measurements in cloudy regions cannot be used in most cases. Therefore the data record created from HIRS measurements has a clear-sky or dry bias due to the fact that cloudy regions are associated with high humidity [*Lanzante and Gahrs*, 2000]. An additional problem may be contamination by very thin cirrus clouds in nominally clear areas [*Berg et al.*, 1999].

[8] The problem of clear-sky bias in UTH data sets can be overcome, or at least significantly reduced, by using microwave measurements [*Buehler et al.*, 2007]. Continuous UTH measurements from microwave instruments on board satellites have been available since 1994. Currently there are three operational microwave instruments measuring UTH: the Special Sensor Microwave (SSM/T-2) on board the DMSP satellites, the Advanced Microwave Sounding Unit B (AMSU-B) on board the NOAA 15, 16, and 17 satellites, and the Microwave Humidity Sounder (MHS) on board the NOAA 18 and the MetOp A satellite. Since we will be frequently mentioning the different NOAA satellites, they will henceforth be referred to as N15 to N18, respectively. For practical reasons, since the data were at hand, only the AMSU-B measurements are used in the current study.

[9] Several authors [e.g., *Rosenkranz*, 2001; *Jimenez et al.*, 2005] have demonstrated the possibility to retrieve humidity from AMSU-B measurements. However, to our best knowledge there is no published study on the climatology of UTH from AMSU-B measurements, and no publicly available AMSU based UTH data set.

[10] This article focuses on describing the properties of such a data set, which we are making available to the scientific community. The article is organized as follows: section 2 describes the method of estimating UTH from AMSU-B measurements, the cloud filtering method, and the gridding of the data. section 3.1 describes the properties of the new data set. It discusses the UTH climatologies (section 3.1), intersatellite differences (section 3.2), the uncertainty introduced by clouds and surface effects (section 3.3), and seasonal UTH variations (section 3.4). Section 4 presents and discusses the comparison of the AMSU UTH to other important data sets of UTH. Finally, section 5 gives summary, conclusions, and outlook.

2. Methodology

[11] The UTH data set described here was derived from AMSU-B measurements from three different NOAA satellites, N15 to N17. AMSU-B is a cross-track scanning, passive, total power microwave radiometer. It has two channels centered at 89 and 150 GHz, respectively, and three channels centered around the water vapor line at 183.31 GHz [*Saunders et al.*, 1995]. All channels work in double sideband mode. The details of the channels are summarized in Table 1. Note, that the values of the noise equivalent temperature (NEΔT) are from the first flight model, not from the instruments currently operating. Furthermore, the actual noise values differ slightly between the three AMSU instruments used here.

[12] The instrument has a swath width of approximately 2300 km, with 90 individual measurement pixels along the swath. The nadir viewing angle for the two innermost scan positions is 0.55°, for the two outermost scan positions it is 48.95°. Because of the Earth's sphericity, this corresponds to incidence angles of 0.62° for the innermost scan positions and 58.5° for the outermost scan positions. The target area size of the measurements at nadir and at the outermost scan position is 20×16 km^2 and 64×52 km^2, respectively. The orbit characteristics and launch times of the different NOAA satellites are summarized in Table 2.

[13] We used level 1b data from the Comprehensive Large Array-data Stewardship System (CLASS). They were converted to level 1c data (brightness temperatures for each AMSU-B pixel) with the ATOVS and AVHRR Processing Package (AAPP), which is briefly described by *Atkinson and Whyte* [2003]. The time period of data used varied from satellite to satellite and is shown in Table 2. For N15, data are available from January 2000. Although N15 was launched in 1998, data recorded before January 2000 have

Table 2. Characteristics of the Different NOAA Satellites[a]

Satellite	Equator Cross. Time	Mean Alt., km	Launch Date	Data Used From
N15	05:58 a.m./p.m.	807	May 1998	Jan 2000
N16	02:11 a.m./p.m.	850	Sep 2000	Oct 2000
N17	10:24 a.m./p.m.	810	Jun 2002	Aug 2002
N18	01:55 a.m./p.m.	854	May 2005	not used

[a]All satellites are polar-orbiting on a sun-synchronous orbit. (Information is taken from the WMO Space Program web page at http://www.wmo.ch/web/sat/POLpresent.html.)

been excluded due to the radio frequency interference problems that the AMSU-B on this satellite had at the beginning [*Atkinson*, 2001]. For the instruments on board N16 and N17, the data coverage starts in October 2000 and August 2002, respectively. The data sets of all three instruments currently reach until February 2007.

[14] The method described by *Buehler and John* [2005] was used to retrieve UTH from microwave measurements. It defines UTH as the relative humidity with respect to liquid water, weighted by the AMSU-B Channel 18 Jacobian. The Jacobian used is the derivative of the brightness temperature with respect to the water vapor volume mixing ratio in fractional units (see the above paper for more details).

[15] The peak altitude of the AMSU-B Channel 18 Jacobian is similar to the Jacobian near 6.3 μm, which is the wavelength commonly used to derive IR UTH products. Hence our UTH and IR UTH are comparable, but not numerically identical. Both IR and microwave UTH corresponds roughly to the mean relative humidity between 500 and 200 hPa.

[16] These UTH products are radiances scaled to a more intuitive unit. The scaling is given by

$$\ln(\text{UTH}) = a + bT_b, \qquad (1)$$

where UTH is the Jacobian-weighted mean of the fractional relative humidity in the upper troposphere, ln() is the natural logarithm, T_b is the Channel 18 radiance expressed in brightness temperature, and a and b are constants. The constants a and b have been determined by *Buehler and John* [2005] by linear regression for a diverse atmospheric profile data set. The coefficients themselves are not repeated here, but note, that a brightness temperature difference of 1 K corresponds to a relative change in UTH of approximately 7%.

[17] According to the simulations by *Buehler and John* [2005], the accuracy of this method should be 2%RH and 7%RH at low and high UTH values, respectively. This is the accuracy of the scaling method, compared to the true Jacobian-weighted mean UTH. It includes the uncertainty due to radiometric noise, but not the uncertainty due to any systematic biases of the AMSU instruments. To assess the latter is difficult, because of the lack of high quality validation data sets. Comparisons of AMSU-B data to radiosondes [*Buehler et al.*, 2004; *John and Buehler*, 2005] showed good agreement for carefully calibrated reference radiosondes, but not surprisingly less good agreement for the global operational radiosonde record. A cross-comparison with AIRS humidity measurements is probably more suited for validation. Such a study is currently in progress.

[18] Measurements from all AMSU-B viewing angles were used to obtain good spatial coverage. This requires viewing angle dependent scaling coefficients for equation (1) that are available by *Buehler and John* [2005]. Since the Jacobians for the different angles are not identical, the altitude weighting for the UTH from the different viewing angles is slightly different. However, the resulting differences in the UTH climatology are very small if the correct coefficients are used, as demonstrated by *John et al.* [2006, Figure 6].

[19] When using data from different viewing angles, scan-dependent instrumental biases need to be mitigated. This was investigated for the three AMSU instruments that are used here by *Buehler et al.* [2005b], with the conclusion that these biases are below approximately 0.5 K for the instruments on N16 and N17, but up to approximately 2 K for the instrument on N15. At that level, scan dependent biases are not expected to affect the total UTH climatology significantly, except perhaps for N15, where the relative error in UTH related to scan bias could reach a few percent.

[20] Microwave humidity data are affected by two contaminations: clouds and surface influence. Clouds can affect measurements if they are high enough to be seen by Channel 18 and if they contain a sufficient amount of ice. The surface can affect measurements if the atmosphere is so dry that Channel 18 sees the surface, which happens at total column water vapor below 3 kg/m^2 [*Buehler et al.*, 2007]. This usually only occurs at high latitudes or in high mountain regions. The effect is strongest where the surface emissivity is low, for example in snow covered areas.

[21] *Buehler et al.* [2007] also showed that a simple filter, combining a threshold on the Channel 18 brightness temperature with a threshold on the Channel 20-18 brightness temperature difference, can reliably screen out both cloud and surface contamination. It is important to note that clouds affect microwave measurements significantly less than IR measurements. Channel 18 usually only detects clouds with an ice water path (IWP) of several hundred g/m^2 (compare *Buehler et al.* [2007, Figure 4].

[22] For midlatitudes, *Buehler et al.* [2007] found that both the cloud wet bias and the cloud filtering dry bias in a microwave UTH climatology are modest. Figures in this paper show cloud filtered data unless stated otherwise. The impact of cloud filtering on the data is discussed in detail in section 3.3.

[23] UTH was derived from the Channel 18 radiance for each AMSU-B pixel. These data were collected for time periods of one month in 1.5° × 1.5° latitude-longitude grid cells. Optionally, the cloud filter of *Buehler et al.* [2007] was applied to each pixel, and the pixel discarded if the filter indicated cloud contamination. We stored both the cloud-filtered and the unfiltered data set. For both data sets, various statistical parameters (number of measurements, median, mean, standard deviation) were calculated for each month and grid cell. Data from different satellites were stored separately. The result is a monthly climatology with 1.5° × 1.5° spatial resolution. The number of UTH values that contribute to the statistics in each grid cell varies, but is of the order 3000.

[24] The data set was restricted to the area between 60°S and 60°N, since at higher latitudes the data are too contaminated by surface contributions, due to the low column water vapor values in these regions. All the data are freely available on the Web site http://www.sat.ltu.se.

3. Data Set Properties

[25] In the following subsections we will discuss some general features of the new data set. We will start with the UTH median climatology, then discuss intersatellite differences, uncertainties due to clouds and surface contributions, and finally seasonal variations in the data.
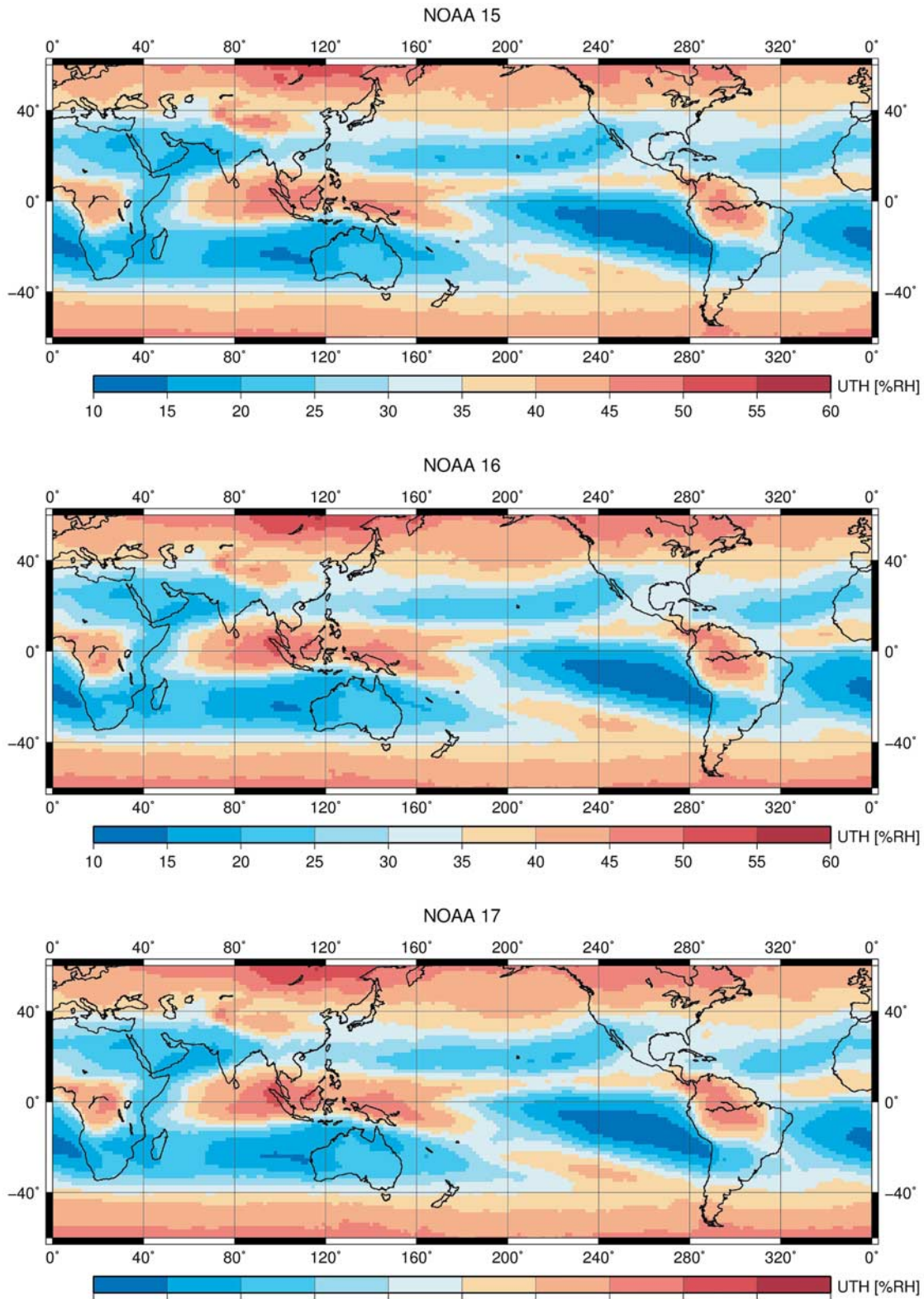
Figure 1. UTH retrieved from different NOAA satellites. (Medians of the monthly medians.) From top to bottom: N15, N16, and N17. Time period of data used is August 2002 to July 2006.

3.1. UTH Median Climatology

[26] To estimate the median climatology, the available data sets were restricted to the common time period August 2002 to July 2006, when all three instruments were operational. This time period was chosen in order to allow a direct comparison between the instruments on different satellites. Figure 1 shows maps of the median of the monthly medians

of retrieved UTH for each of the three satellites. We show the median instead of the mean here, as this was found by *John et al.* [2006] to be more appropriate for UTH, due to the non-Gaussian nature of the UTH distribution. The maps for all three instruments are very similar. The common features will be discussed here, whereas the differences will be discussed in the next section.

[27] The distributions obtained for all three AMSU-B instruments reflect the prevailing distribution of UTH, determined by the general circulation. In interpreting the plots, it is important to keep in mind that UTH is a measure of relative humidity, not absolute humidity. Thus regions of subsidence are marked by low UTH, because sinking air warms adiabatically, and relative humidity decreases accordingly. In contrast to this subsidence drying, regions of ascent are marked by high UTH. When the air rises, temperature drops adiabatically, and relative humidity increases accordingly until the saturation point is reached. Further ascent is moist-adiabatic, with humidity staying at the saturation point, and excess-moisture being converted to condensate. This is an over simplification, because it neglects both the details of condensate nucleation, and the possible presence of super saturation, particularly with respect to ice. Nevertheless, it describes the global picture quite well.

[28] At low latitudes, in the tropics and subtropics, the dominating global circulation pattern is the overturning Hadley circulation. As expected, regions with deep convection in the intertropical convergence zone (ITCZ) exhibit high UTH, close to saturation with respect to ice. (Note that $100\%RH_i$ (relative to ice) occurs significantly below $100\%RH$ (relative to liquid water) at low temperatures. At 250 K, ice saturation is reached at approximately $80\%RH$, at 220 K it is reached at approximately $60\%RH$.) In contrast to the regions of ascent, the subsidence regions in the descending branch of the Hadley circulation in the subtropics exhibit low UTH. This general meridional pattern is clearly visible in Figure 1.

[29] Additionally, the figure also shows zonal patterns. In the band with high UTH around the ITCZ, there are three areas with pronouncedly high humidity: one over central Africa, one over the maritime region between South Asia and Australia, and one over Central America. All three regions are associated with the strongest convective systems inside the ITCZ, transporting large amounts of air (and moisture) to the upper troposphere.

[30] Similarly strong zonal variations can be found in the subsidence areas. Regions with particularly low UTH in Figure 1 are located in the subtropics in the eastern regions of the oceans, particularly in the North and South Pacific and the North and South Atlantic. Here zonal circulations, such as the Walker circulation in the equatorial Pacific Ocean, are superimposed onto the meridional circulation systems. In general, the low humidity patches are drier in the Southern Hemisphere than in the Northern Hemisphere.

[31] Besides the wet band in the ITCZ, wet bands can also be found at midlatitudes approximately between $40-60°$ in both hemispheres. These bands are due to wave activities in the midlatitudinal west wind zone with the associated weather and wind systems [*Bates and Jackson*, 2001]. The highest UTH values over Northeast Asia near 60°N should be considered with caution, since this area is affected by surface contamination in winter (more on this in section 3.3). Applying the surface and cloud contamination filter can have moist-biased the UTH statistics in this area, because surface contamination occurs when the atmosphere is very dry.

[32] The median distribution of UTH obtained from the AMSU-B instruments is broadly consistent with the global humidity distribution observed by other instruments. For example, it is consistent with the distribution reported by *Soden and Bretherton* [1996] for the time period 1981–1991 using TOVS data and with that of *Bates and Jackson* [2001] for the time between 1979 and 1998 using HIRS data. Both these other instruments retrieve UTH from infrared data using the 6.7 μm water vapor band. *Gettelman et al.* [2006] present relative humidity results from IR instrument AIRS for a layer between 250 and 200 hPa. Although these results cover only the upper levels of the UTH product provided from AMSU$-$B, the observed patterns and the seasonal variation are in agreement.

3.2. Intersatellite Differences in UTH

[33] Although the distributions of UTH in Figure 1 all appear to be similar, there are differences between the instruments on different satellites. Figure 2 shows these differences for one month of data, August 2006. N16 is taken as the reference, the top row shows the difference for N15, the bottom row for N17. The left column shows maps of the relative difference. These plots reveal that UTH from N15 is systematically drier than UTH from N16. On the other hand, N17 and N16 are in much closer agreement. An area-weighted average over all grid points yielded mean relative differences of -3.4% for N15 and $+1.0\%$ for N17, relative to N16. (The area-weighted mean was calculated by weighting each grid point with the cosine of the latitude. The values are practically identical to unweighted averages over all grid points.) This implies that the N15 brightness temperatures are somewhat warmer than those from N16 and N17. The standard deviations associated with the mean relative differences are encouragingly low, approximately 5% for N15 and approximately 6% for N17.

[34] The right column of Figure 2 shows scatterplots of UTH(N15) and UTH(N17) versus UTH(N16). These plots reveal a very high correlation with a correlation coefficient of 0.99 in both cases. The maximum scatter occurs at UTH values near 40%RH.

[35] In the scatterplot for N15 versus N16, the dashed line showing the linear fit is clearly off the ideal diagonal for high UTH values, while it appears to be close to the diagonal for low UTH values. This suggests an absolute radiance warm bias for N15 as the source of the discrepancy, because such a bias directly leads to a relative dry bias in UTH, due to the logarithm in equation (1).

[36] In addition to the large-scale biases, the relative difference maps also show pronounced spatial patterns. These patterns in the N15 and N17 plots are highly correlated, which makes it likely that they are related to spatial and temporal sampling differences between N16 and the other two satellites. Most significant here is that the observations are made at different local times (see Table 2). The diurnal cycle in UTH and high reaching clouds [e.g., *Tian et al.*, 2004; *Chung et al.*, 2004, 2007] may explain
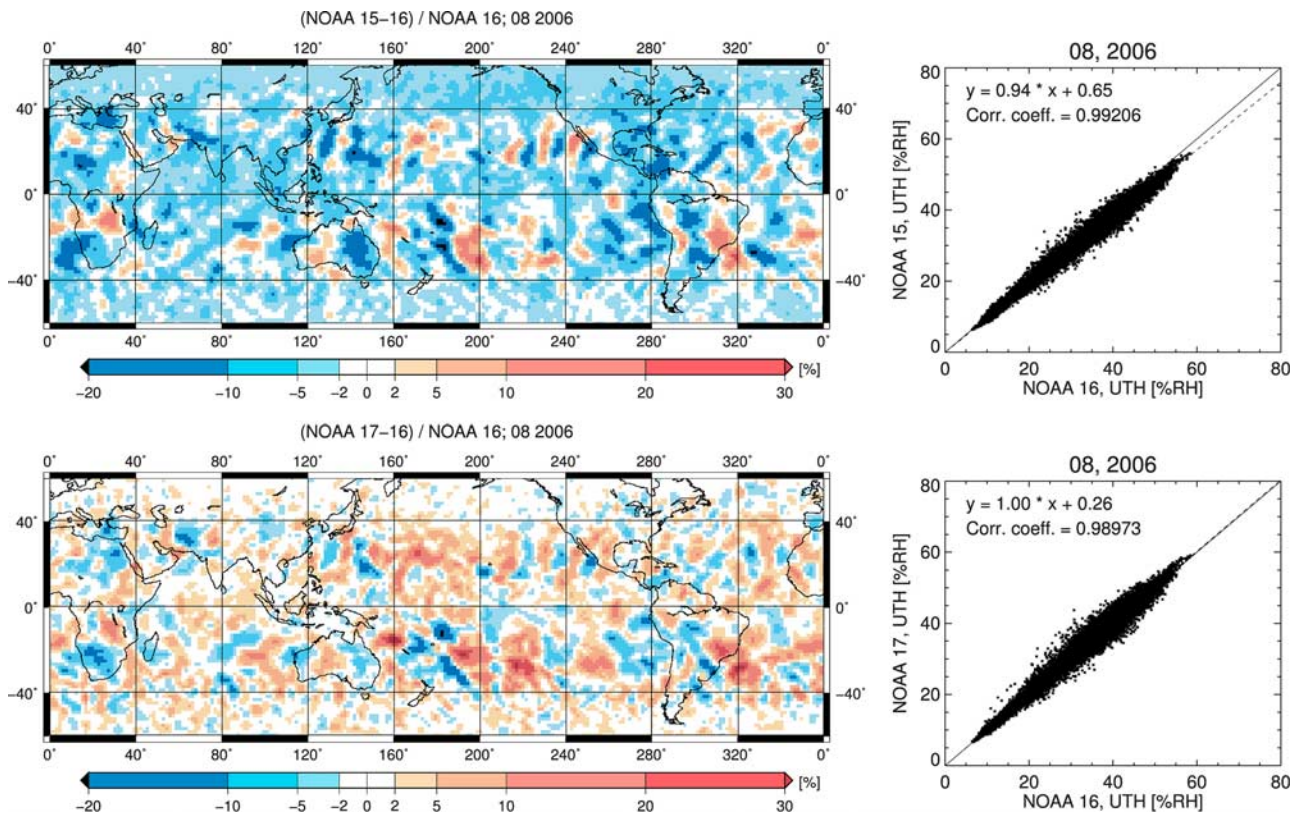
Figure 2. Differences in gridded UTH for August 2006 between the AMSU-B instruments on different satellites. The left column shows maps of the relative difference. Top: [UTH(N15) − UTH(N16)]/UTH(N16), Bottom: [UTH(N17) − UTH(N16)]/UTH(N16). The right column shows scatterplots. The dashed lines in the scatterplots are linear fits.

some of the patterns found. Indeed, useful information on the diurnal cycle could potentially be extracted from these patterns.

[37] It is important to check, whether the biases between the different AMSU-B instruments are constant, or whether they drift with time. As a measure for the bias we take, once again, the area-weighted mean relative difference. Figure 3 shows the time evolution of that quantity for N15-N16 (top) and N17-N16 (bottom). The error bars show the associated standard deviations. The standard deviations for both sensors are similar and do not change much from month to month. The standard deviation value is approximately 7%.

[38] The N15-N16 bias varies slightly, without a clear trend. Relative difference values in UTH are around −2% to −4%, corresponding to a radiometric offset of +0.3 K to +0.6 K according to equation (1). The N17-N16 bias has drifted during the operation time of N17 from approximately −1% (+0.1 K radiometric offset) to +2% (−0.3 K radiometric offset). The reason for this drift is unclear.

[39] To summarize this section, we find that there are both sampling and instrumental differences in UTH between the different AMSU-B instruments. They have means (biases) of below 4% relative error and standard deviations of approximately 7%. The sampling differences could be due to temporal aliasing from insufficiently resolving the diurnal cycle of humidity and clouds.

[40] The instrumental differences appear to be due to radiometric offsets. To put these results into perspective
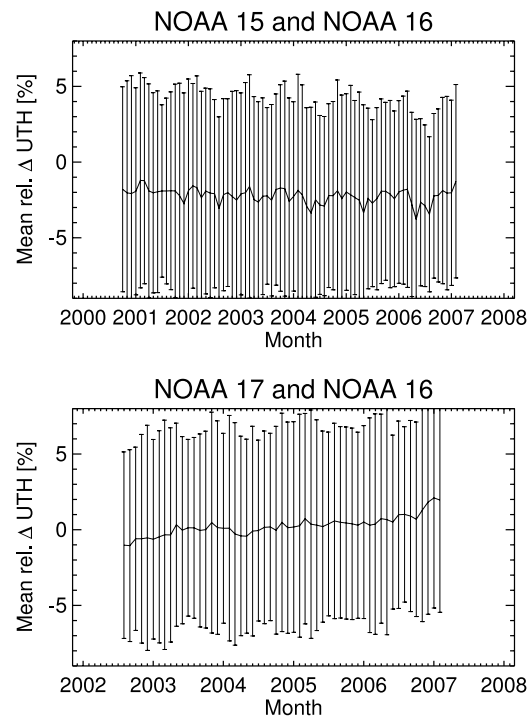
Figure 3. Time evolution of UTH biases. Shown is the time evolution of the area-weighted mean relative difference for N15−N16 (top) and N17−N16 (bottom). Error bars show the standard deviations associated with these means.

one should note that these discrepancies are comparable in magnitude to the uncertainty that is introduced by clouds (see next section), and small in comparison to the large discrepancies that generally persist between different UTH data sets. For example, *Soden et al.* [2004] have documented discrepancies between radiosondes and IR satellite measurements of 40% relative difference in UTH and *John and Soden* [2007] reported that climate models show up to 100% relative difference in upper tropospheric water vapor with respect to AIRS observations.

3.3.   Impact of Clouds and Surface Contributions

[41]   As documented for example by *Greenwald and Christopher* [2002] and *Buehler et al.* [2007], high ice clouds can affect microwave UTH measurements. Furthermore, surface contributions can affect microwave UTH measurements for very dry atmospheres. The cloud and surface filter, that was developed by *Buehler et al.* [2007], was therefore applied to the data, as explained in section 2. Results shown so far were for the filtered data. Here, we discuss the uncertainty that is introduced into the UTH climatology by the filtering procedure.

[42]   Figure 4 shows the differences between the unfiltered and the filtered median UTH for N16 and four different months. The months January 2006, April 2006, July 2006, and October 2006 were chosen to represent the different seasons. Clouds mostly introduce a wet bias, because the cloud signal is interpreted as additional moisture for unfiltered data. In the case of surface effects, which occur at midlatitudes in the winter season, there can be dry or wet biases, depending on humidity profile and surface type.

[43]   Our recommendation is to use Figure 4 as an uncertainty estimate for the UTH data, particularly for Figure 1 and for Figure 5. From the case studies that were carried out by *Buehler et al.* [2007], one can expect the true all-sky UTH median and mean values to be between the filtered and the unfiltered microwave UTH values. The uncertainty introduced by clouds is up to approximately 10%RH in areas with strong convection. Surface contamination in midlatitude winter can introduce even larger uncertainties, therefore the midlatitude winter data should only be used with caution.

[44]   Note, that the cloud uncertainty quoted above is for the gridded monthly mean data, not for individual AMSU pixels, where the uncertainty can be much higher. If one takes that into account, then our results are roughly consistent with those of *Greenwald and Christopher* [2002], who found that nonprecipitating clouds produce on average 5%RH error in UTH retrievals, and precipitating clouds produce on average 18%RH error. This comparison is discussed further by *Buehler et al.* [2007].

[45]   To summarize, there are nonnegligible uncertainties in microwave UTH data due to cloud and surface effects. Nevertheless, microwave data allow a much closer guess for the true all-sky UTH climatology than IR data, since the number of cloud cases that affect the microwave measurements is lower. The simple approach to use filtered and unfiltered data as estimates for the uncertainty range is not possible for IR data, due to their stronger sensitivity to clouds.

3.4.   Seasonal Variations in UTH

[46]   To show the seasonal cycle of UTH, we use the same four months that were used in the previous section: January 2006, April 2006, July 2006, and October 2006. Figure 5 shows the monthly median UTH for these four months from N16. In January (top plot) the low humidity belt related to the subsiding branch of the Hadley circulation is stretched all through the subtropics in the Northern Hemisphere reaching close to the equator over eastern Africa and the central and eastern Pacific, only interrupted by two narrow regions of high humidity stretching to higher latitudes west of America and across northern Africa. In the dry branches, UTH is less than 35%RH. The driest values of UTH are found in the central part of the northern Pacific and over the Arabian Sea with values below 10%RH.

[47]   In the Southern Hemisphere, the low humidity values associated with the subsiding branch of the Hadley circulation are not as evenly distributed zonally as in the Northern Hemisphere, with several bands of increased humidity extending into midlatitudes. The driest regions in the Southern Hemisphere are found over the oceans close to the continental coastlines, in the South Pacific along the South American coastline, and in the South Atlantic along the African continent with values down to 10%RH. In the Indian Ocean, close to the Australian coastline, UTH values reach down below 10%RH.

[48]   The ITCZ is located at its southernmost position in January, south of the equator, with UTH maxima of 50–55%RH over central South America, southern Africa, and Indonesia.

[49]   The northern midlatitude values for UTH are very high, especially over the large land areas in northern Canada and northern Russia, where the continental climate leads to very low temperatures and correspondingly low total column water vapor. A check with Figure 4 reveals that these values cannot be trusted, as they are strongly influenced by surface contributions.

[50]   In April (second plot in Figure 5) the humid ITCZ has moved northward except over the Atlantic. It is now situated around the equator with decreased UTH. The dry northern subtropical band has weakened and in some areas shifted toward lower latitudes. Other patterns found in January are still visible in April, but both the dry and wet extremes have decreased in amplitude.

[51]   In July (third plot in Figure 5) the southern subtropics are dominated by a closed belt of low humidity. Lowest UTH values are observed in the Indian Ocean and in the East Pacific. The highest UTH values appear east of India and can be related to the Indian Monsoon. The band with high UTH marks the shift of the ITCZ to a position north of the equator. In the Northern Hemispheric subtropics there are two distinct patches of low UTH. One stretches from the Atlantic over North Africa to central Asia. This patch has its lowest UTH values below 10%RH in the region between the north of the Arabic Peninsula and northern Egypt. A second patch with less extreme low UTH values is located at the east side of the Pacific close to North America.

[52]   In October (bottom plot in Figure 5) the moist ITCZ has moved slightly southward again and both dry and wet extremes have decreased in amplitude. The low humidity belt in the southern subtropics is interrupted by narrow
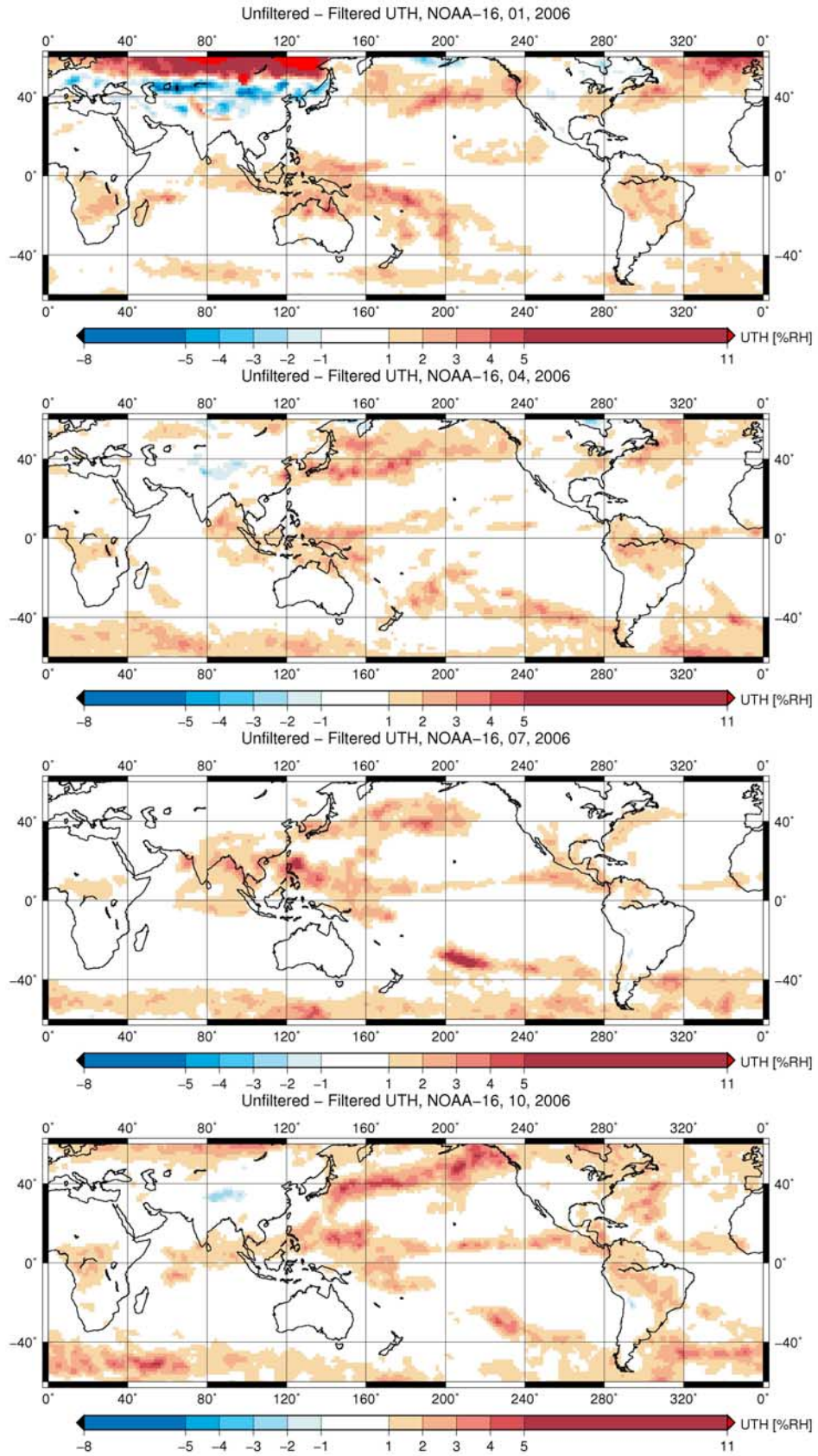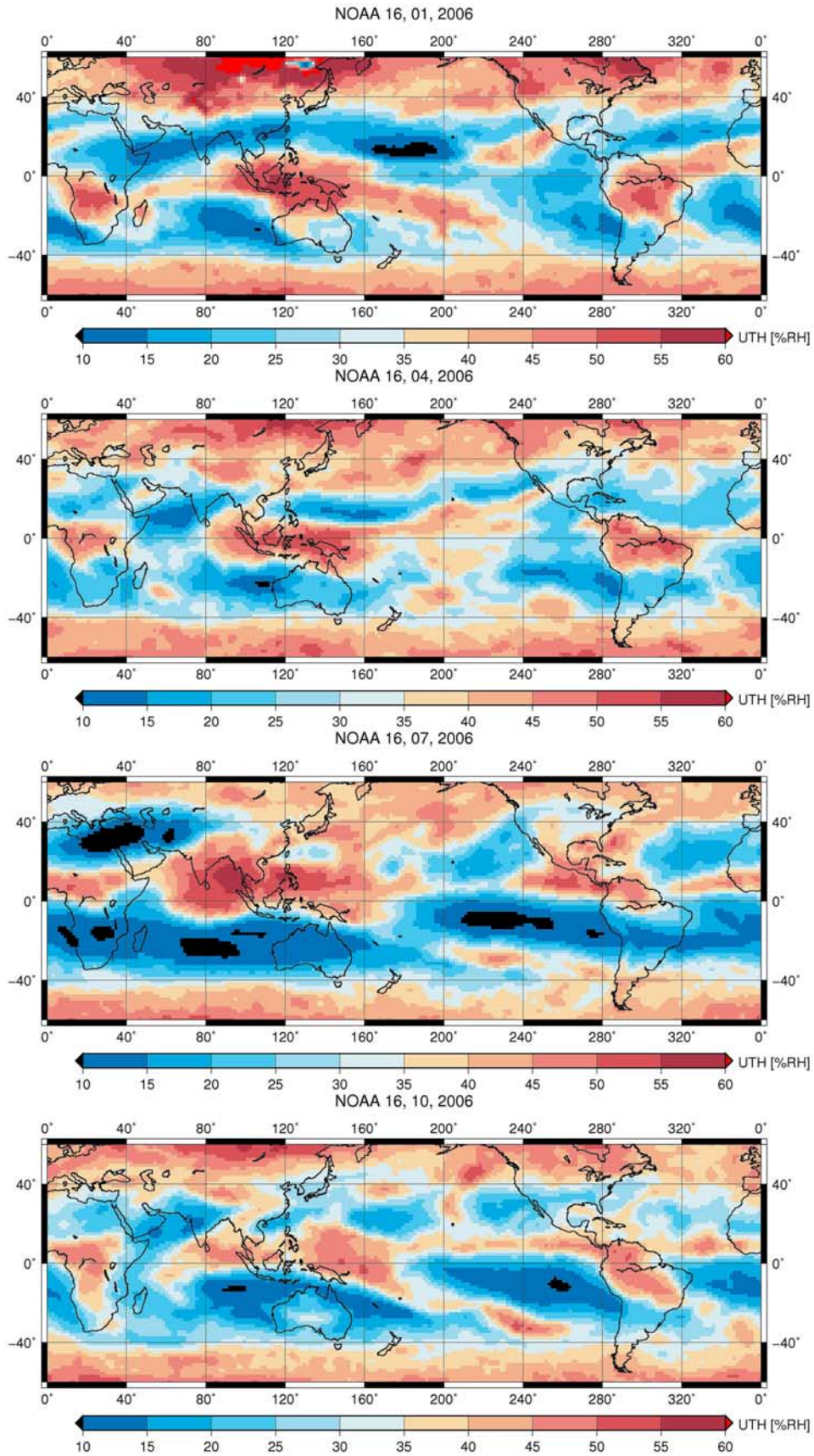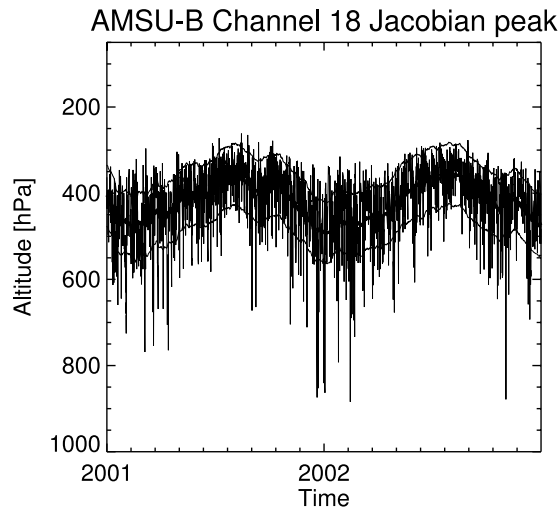
Figure 4. Differences between the unfiltered and the filtered median UTH for N16 and four different months, January 2006, April 2006, July 2006, and October 2006.

BUEHLER ET AL.: UTH FROM MICROWAVE SENSORS

Figure 5. Monthly median UTH for N16 and four different months, January 2006, April 2006, July 2006, and October 2006.

Figure 6. AMSU-B Channel 18 Jacobian peak altitude calculated with the Atmospheric Radiative Transfer Simulator (ARTS) from Lindenberg radiosonde data for 2001–2002. The "noisy" line shows the time evolution of the individual radiosonde measurements. The heavy line shows the same, but smoothed with a 30-d boxcar filter, in order to bring out the seasonal cycle more clearly. Thin lines above and below the heavy line show the standard deviation of the individual measurements, relative to the smoothed heavy line.

regions of high UTH reaching from the ITCZ to southern midlatitudes, mainly over the continents.

[53] The results on the seasonal variation of UTH are broadly consistent with the results reported by *Chen et al.* [1999, Plate 1] who investigated the seasonal variations in MLS humidity and cloud data. This is despite the fact that the data used there were for 215 hPa, whereas our data approximately are an average over the altitude region between 500 and 200 hPa.

3.5. Variations in AMSU-B Sounding Altitude

[54] As mentioned in section 2, and as discussed in more detail by *Buehler and John* [2005], the UTH definition as a Jacobian-weighted mean relative humidity implies that the actual altitude, over which the mean is taken, varies slightly for different atmospheric situations. This is not only true for the AMSU UTH product, but also for similar IR UTH products, such as those described by *Soden and Bretherton* [1996] and *Jackson and Bates* [2001].

[55] Figure 6 illustrates this variation by showing how the Jacobian peak altitude changes during the course of 2 years for a midlatitude location (DWD reference station Lindenberg at approximately 52°N, see section 4.2 for exact position). The figure was generated by calculating the peak of the AMSU-B Channel 18 Jacobian based on radiosonde profiles of temperature and humidity, which are available four times per day. The program used to calculate

the Jacobians was the Atmospheric Radiative Transfer Simulator (ARTS) [*Buehler et al.*, 2005a].

[56] The seasonal cycle in peak altitude has an amplitude of approximately 100 hPa around a mean value of approximately 450 hPa. The seasonal curve was obtained by smoothing the individual measurements with a 30-d boxcar filter.

[57] For individual measurements, the standard deviation of the fluctuations in Jacobian peak altitude around the smoothed seasonal curve is only 71 hPa. This means, although extreme peak altitudes as low (in altitude) as 800 hPa are possible in rare cases, the AMSU measurement is generally observed at the same altitude. The rare outlier cases are those cases when the atmosphere is extremely dry. Both the occurrence of these outlier cases, and the seasonal cycle itself, should be less pronounced closer to the equator than for this midlatitude location, which is close to the northern latitude limit of the UTH data set.

[58] Although the variations in sounding altitude are not very large, the recommended way to compare this kind of UTH data set to a climate model is to simulate microwave radiances for the model fields and scale them to UTH, using the scaling coefficients by *Buehler and John* [2005]. Fast radiative transfer models to calculate the radiances are openly available, e.g., RTTOV [*Saunders et al.*, 1999].

4. Comparison to Other Related Data Sets

[59] The purpose of this section is to provide an initial validation of the new AMSU UTH data set. We present and discuss comparisons to IR satellite data (HIRS and, very briefly, AIRS) as well as to radiosonde (RS) data. All the AMSU data used in this section are from N16.

[60] In the comparison, we mostly look at three statistical parameters: the mean difference (in %RH), the standard deviation of the difference (in %RH), and the correlation coefficient (absolute number). We frequently refer to the mean difference as "bias".

4.1. Global Comparison to Infrared Satellite Data

[61] Figure 7 shows a comparison of the mean field for 2 years of AMSU and HIRS UTH data. The HIRS UTH data are from the satellite N14 and were produced with the algorithm of *Soden and Bretherton* [1996]. As the figure shows, the HIRS data has a dry bias against the AMSU data. Its value is approximately −9%RH for the time period 2001−2002. Despite the bias, the two data sets correlate quite well. The standard deviation is approximately 6%RH and the correlation coefficient above 0.8. The exact numbers can be found in Table 3.

[62] *Jackson and Bates* [2001] describe a slightly different algorithm to derive HIRS UTH. We compared AMSU UTH to that data set also, but the result is very similar. The dry bias of that HIRS data set against AMSU is slightly smaller (approximately 7%RH), but the standard deviation associated with the mean difference is somewhat

Figure 7. A comparison of the gridded AMSU UTH data to gridded HIRS UTH data by *Soden and Bretherton* [1996]. Compared is the mean field for the time period 2001−2002. Top: AMSU UTH. Second from top: HIRS UTH, grid cells where data for one or more months are missing are marked in black. Third from top: Difference (HIRS-AMSU) in percent RH. Bottom: Relative difference (HIRS-AMSU)/AMSU in percent.
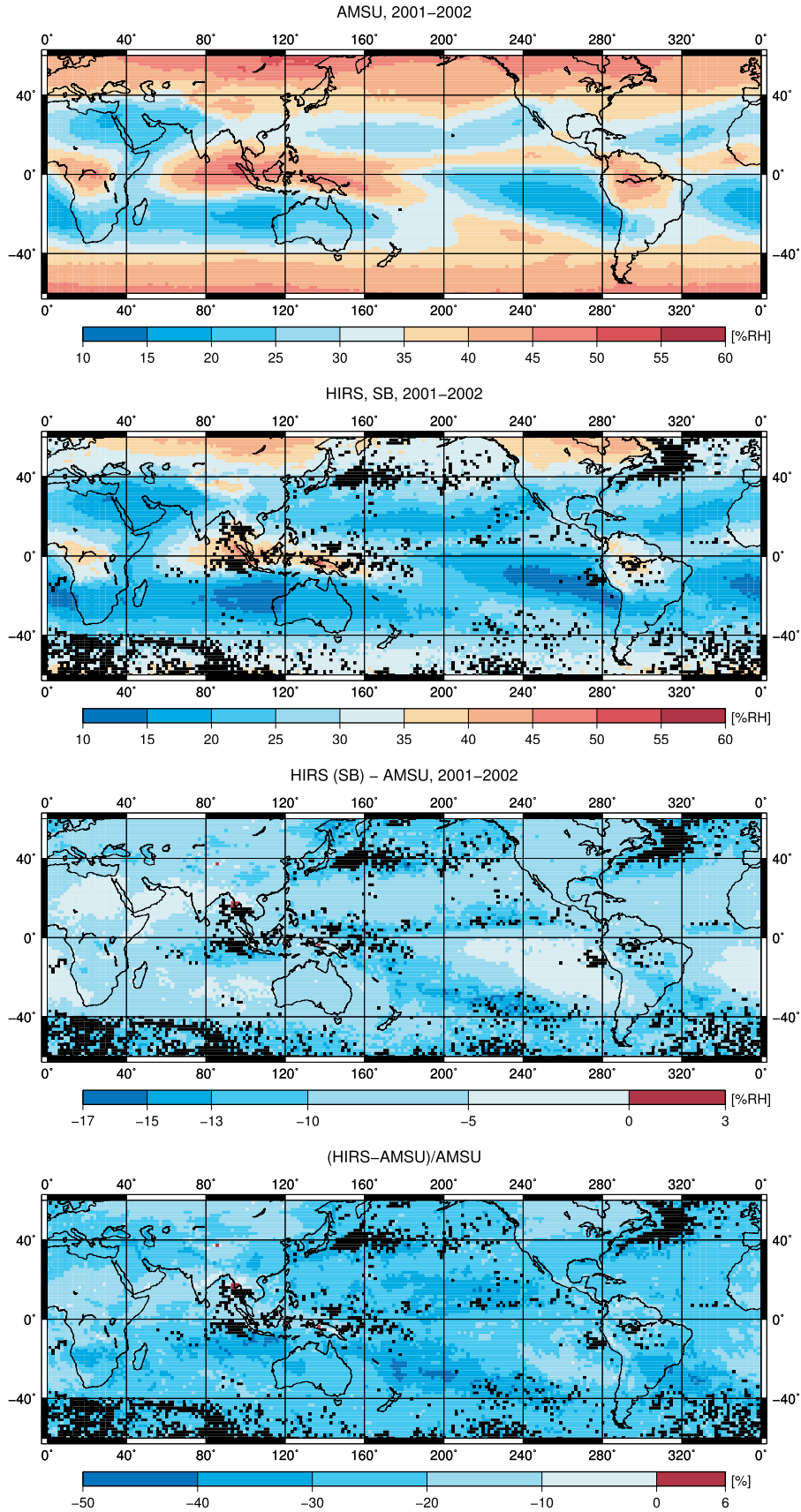
BUEHLER ET AL.: UTH FROM MICROWAVE SENSORS

Figure 7

Table 3. Statistics of the Comparison to Other Data for the Time Period 2001–2002[a]

Data Set	Mean Diff., %RH	Std. Dev., %RH	Corr. Coeff.
Overall HIRS JB − AMSU	−6.89	6.22	0.81
Overall HIRS SB − AMSU	−8.54	5.70	0.83
Jan 2003 AIRS V5 − AMSU	2.61	3.50	0.96
Jan 2003 AIRS V4 − AMSU	2.22	3.44	0.96
Lerwick AMSU − RS	−4.33	1.68	0.87
Lerwick HIRS JB − RS	−12.69	5.42	0.37
Lerwick HIRS SB − RS	−15.99	4.31	0.43
Lindenberg AMSU − RS	1.56	1.12	0.87
Lindenberg HIRS JB − RS	−5.05	4.82	0.14
Lindenberg HIRS SB − RS	−7.40	2.96	0.57
Gibraltar AMSU − RS	0.17	1.91	0.94
Gibraltar HIRS JB − RS	−4.83	3.81	0.76
Gibraltar HIRS SB − RS	−7.29	3.83	0.76
Tenerife AMSU − RS	4.90	2.78	0.92
Tenerife HIRS JB − RS	0.02	3.89	0.83
Tenerife HIRS SB − RS	−1.50	4.25	0.79
St. Helena AMSU − RS	1.05	1.73	0.91
St. Helena HIRS JB − RS	−1.10	2.39	0.86
St. Helena HIRS SB − RS	−1.37	2.25	0.86

[a]The AMSU data are those from N16. "Mean Diff." is the mean of the difference of the given data sets. "Std. Dev." is the standard deviation of this difference. "Corr. Coeff." is the correlation coefficient between the given data sets. The first 2 rows show the overall agreement between HIRS and AMSU over all 240 × 80 grid cells and all 24 months of the 2 year intercomparison period. The next two rows show the global comparison to AIRS version 5 and version 4 humidity profiles for one month, January 2003. The remaining rows show the comparison of both AMSU and HIRS UTH to radiosonde data in the 2001–2002 time period at the five comparison sites. (24 monthly values are compared in each case.) "HIRS JB" is the HIRS data set described by *Jackson and Bates* [2001], "HIRS SB" is the HIRS data set described by *Soden and Bretherton* [1996]. "RS" means radiosonde. For the global comparisons, AMSU is the reference. For the site comparisons, RS is the reference.

larger (6.2%RH instead of 5.7%RH), and the correlation coefficient is slightly smaller (see Table 3 for all numbers).

[63] We also did a comparison to global AIRS humidity profiles for one month of data, January 2003. The radiative transfer model ARTS was used to simulate AMSU brightness temperatures for the AIRS profiles, which were then processed by the same algorithm as the AMSU data. Two different versions of the AIRS profiles were tested, V4 [*Tobin et al.*, 2006] and the new V5, both obtained from the NASA AIRS homepage at http://daac.gsfc.nasa.gov/AIRS/.

[64] The results of the AIRS comparison are summarized in Table 3 with the other comparison results. The correlation between AIRS and AMSU UTH is very high, above 0.9,

Table 4. Intercomparison Site Locations[a]

Name	Latitude	Longitude	#
Lerwick	60.14°N	1.18°W	2479
Lindenberg	52.21°N	14.12°E	2492
Gibraltar	36.15°N	5.35°W	1416
Tenerife	28.46°N	16.26°W	1397
St. Helena	15.93°S	5.67°W	412

[a]"#" is the number of valid radiosonde launches in the 2001–2002 time period. Valid were launches that provided humidity readings up to at least 200 hPa.

with standard deviations around 4%RH. Compared to AMSU, AIRS V4 has a wet bias of approximately +2.2%RH. AIRS V5 has a slightly larger wet bias of approximately +2.6%RH.

[65] Finally, Figure 8 shows a scatterplot of monthly mean AMSU UTH versus monthly mean high cloud fraction (HFC), estimated from AIRS data [*Kahn et al.*, 2007]. The data used is for the time period 2003–2005. As expected, high UTH correlates with high HCF, the correlation coefficient between the two data sets is 0.68. This appears to be consistent with Figure 7a of *Soden and Fu* [1995], although they used another index for deep convective clouds.

4.2. Local Comparisons to Radiosonde Data

[66] A set of RS stations was selected for the comparison. Selection criteria were coverage of different latitudes, and data availability. The station names and positions are listed in Table 4. The table lists also the number of valid soundings from each station for the 2001–2002 comparison time period. Launches were considered valid if they provided humidity readings at least up to an altitude corresponding to a pressure of 200 hPa.

[67] The comparison method was similar to that for the AIRS data: The radiative transfer model ARTS was used to simulate AMSU brightness temperatures for the RS profiles, which were then processed by the same algorithm as the AMSU data. From these data, monthly mean UTH values were calculated, along with their standard deviations. This was compared to the matching grid cell of the gridded monthly mean AMSU UTH data.

[68] The RS UTH was taken as the reference in the comparison, despite the fact that there are significant biases between the UTH data records at different radiosonde
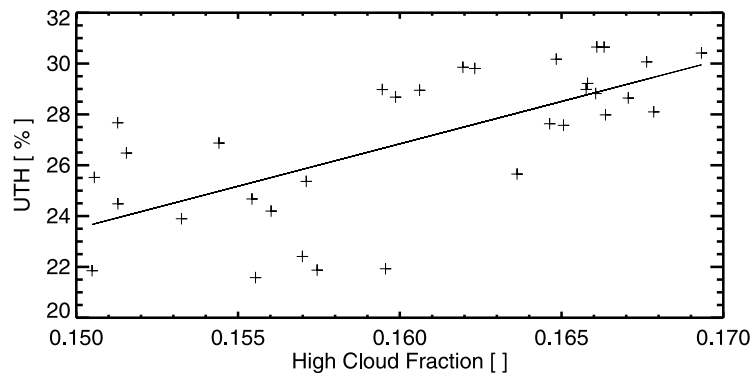
Figure 8. A scatterplot of AMSU UTH versus AIRS high cloud fraction. The straight line is a least squares fit.
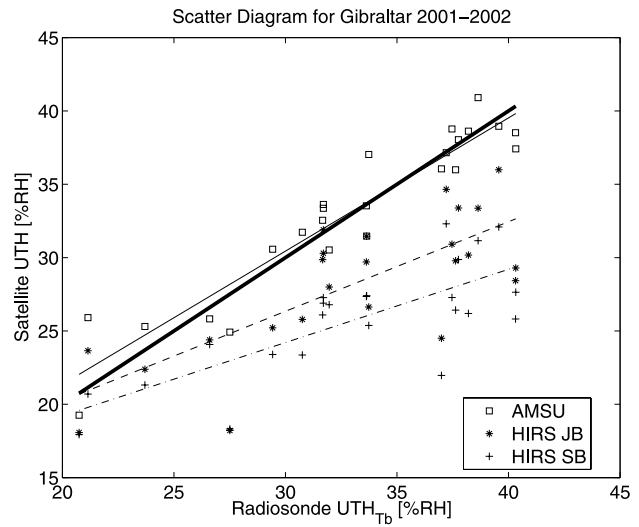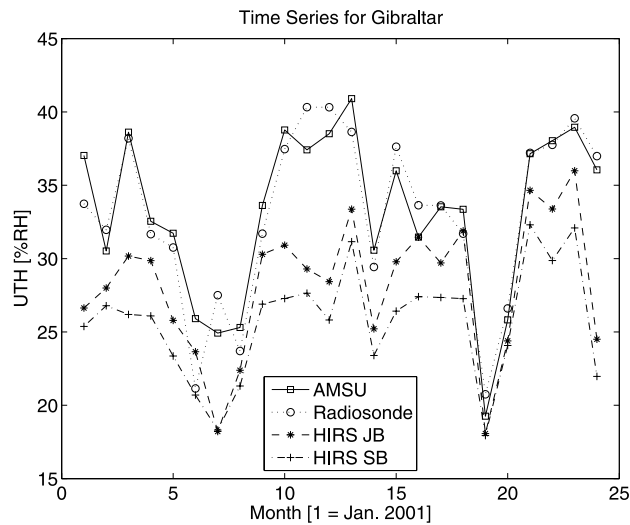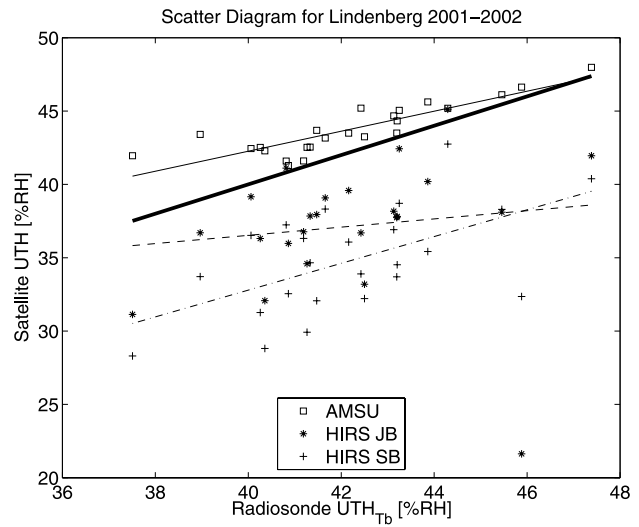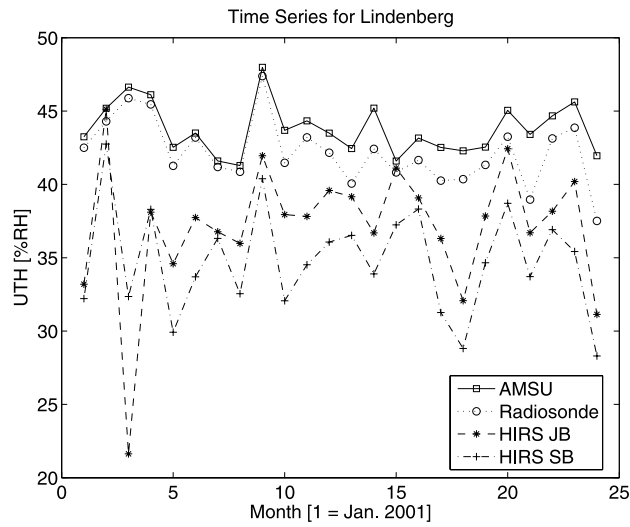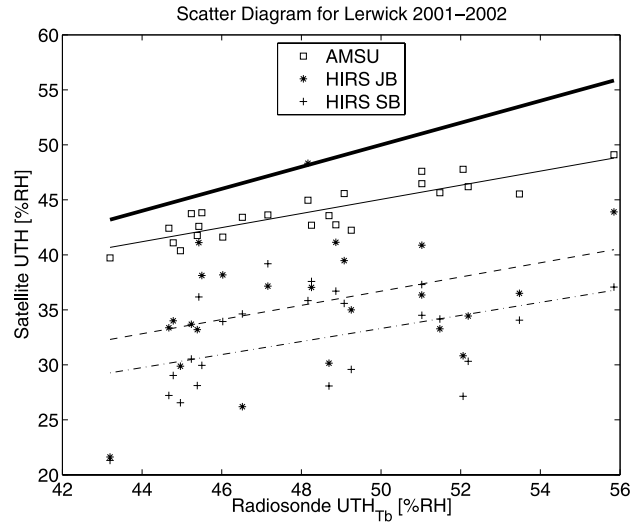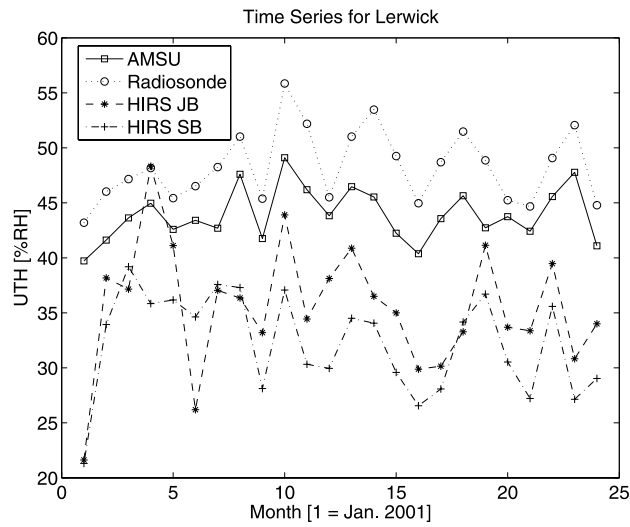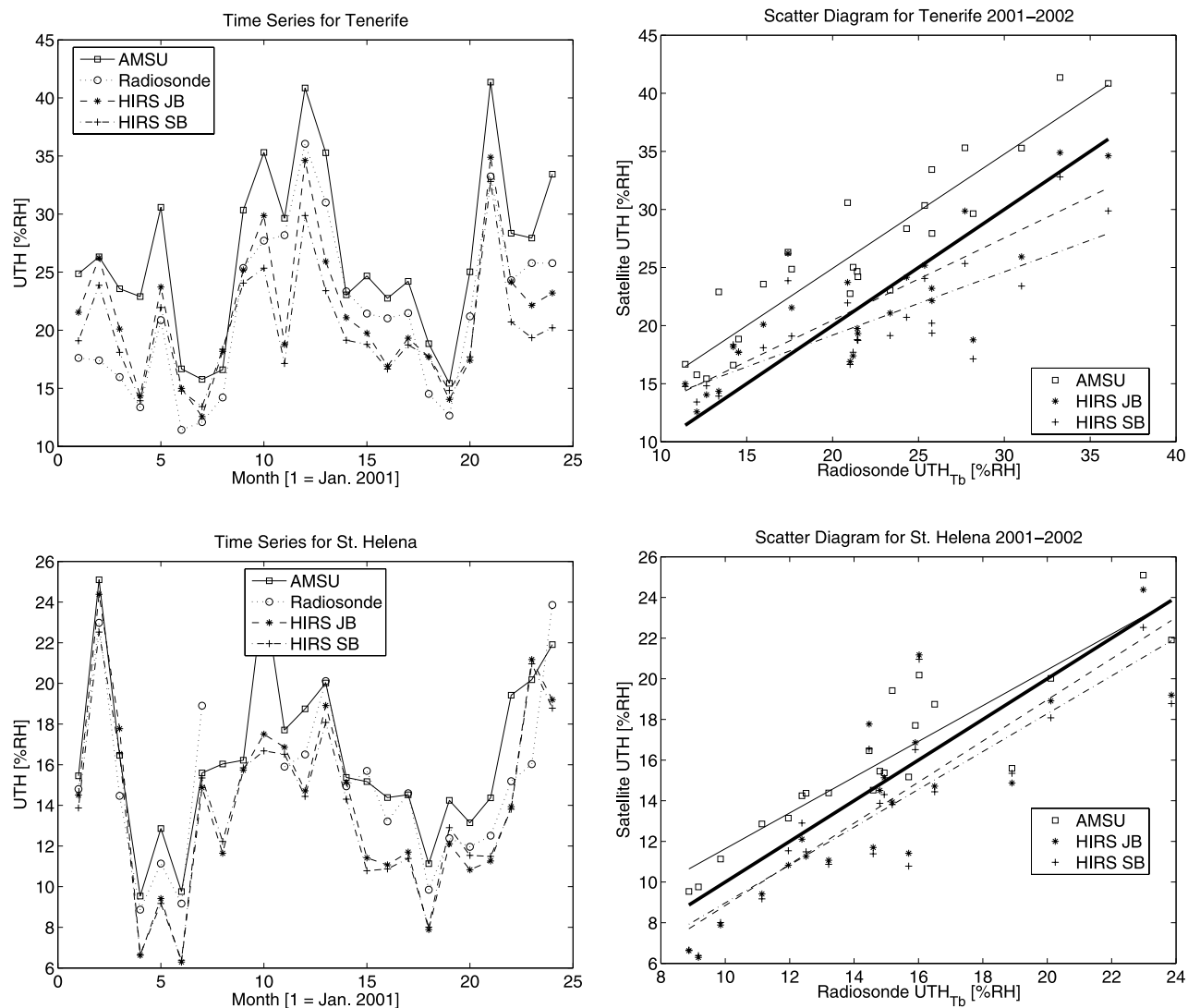
Figure 9. Continued in Figure 10, see caption there.

Figure 10. Figure 9 continued. Comparison of AMSU and HIRS UTH to Radiosonde UTH at the five comparison sites. Compared are monthly mean UTH values for 2001 and 2002. The left column shows time series plots, the right column scatter diagrams. In the scatter diagrams, the bold straight line indicates the diagonal. The other straight lines indicate linear fits, with line styles for the various data sets as in the time series plots.

stations, as discussed for example by *John and Buehler* [2005].

[69] Comparison results are shown in Figures 9 and 10 as both time series plots (left column) and scatter diagrams (right column). The figures show AMSU UTH, as well as both versions of HIRS UTH, in comparison to the RS data.

[70] The agreement between AMSU and RS data at the selected locations is generally good, with biases between −5 and +5%RH, standard deviations below 3%RH, and correlation coefficients above 0.85. (The exact numbers can be found in Table 3.) The AMSU UTH has a slight moist bias against most RS stations, which is consistent with *John and Buehler* [2005]. It is also consistent with *Turner et al.* [2003], who have reported a radiosonde dry-bias of 5% (relative difference) against microwave measurements of column water vapor. That result is for Vaisala RS80-H radiosonde profiles taken by the Atmospheric Radiation

Measurement (ARM) program. Most likely, the RS data used in our comparison is also from Vaisala RS80 type sensors, since they were the prevailing type at the time. We do not calculate an average bias for all stations here, since the RS network is not homogeneous and thus such a number would be misleading.

[71] The HIRS UTH data have a significant dry bias against most RS stations, which is consistent with the findings of *Soden and Lanzante* [1996].

[72] For the station Lindenberg, the variability of the individual data contributing to the monthly means was also investigated, in addition to the monthly mean data. For the radiosondes that is the standard deviation of the approximately 100 UTH values that contributed to each monthly mean, for AMSU it is the standard deviation of the UTH from each individual pixel that fell into that grid cell in the given month. In both cases (AMSU and radiosonde) this

does not change much from one month to the other. The average value is 14%RH for the radiosonde and 12%RH for AMSU. We conclude that the variability within each month is consistent between AMSU and RS.

5. Summary, Conclusions, and Outlook

[73] The purpose of this article is to present and document a new Upper Tropospheric Humidity (UTH) data set, derived from operational satellite microwave data. More specifically, the data set is derived by a simple scaling method from radiances measured by Channel 18 of the AMSU-B sensor, at 183.31 ± 1 GHz.

[74] The data set is freely available on our web page. It consists of monthly maps of UTH on a global $1.5° \times 1.5°$ grid between the latitudes 60° S and 60° N. The instruments used so far are the AMSU-B sensors on the NOAA satellites N15 to N17, which means that the data starts in January 2000. UTH data are available separately for the different sensors.

[75] The definition and properties of this microwave UTH product are largely similar to the UTH product from IR data that has been used by *Soden and Bretherton* [1993] and others. However, a key difference is that microwave radiances are less affected by clouds than IR radiances. Thus microwave data processed with and without cloud filtering can be regarded as error bounds for the true all-sky UTH value [*Buehler et al.*, 2007]. The methodology to derive UTH from radiances has been validated by comparing AMSU-B measurements to radiosondes [*Buehler and John*, 2005; *John and Buehler*, 2005; *Buehler et al.*, 2004].

[76] To give an impression of the new data set, the article discusses its main statistical properties. The global mean distribution of UTH in the data set is in good qualitative agreement with IR UTH climatologies, such as [*Soden and Bretherton*, 1996]. The data set also captures the yearly cycle of UTH, consistently with expectations based on the known features of the general circulation.

[77] UTH Data from different sensors on different satellites are remarkably consistent, with biases below approximately 4% relative difference and standard deviations of approximately 7%. UTH from N15 was found to have a persistent low bias of −2% to −4% relative difference compared to UTH from N16. UTH from N17 was found to have a drifting bias compared to UTH from N16, where the drift was from −1% in August 2002 to +2% in February 2007.

[78] An initial validation of the new data set against IR satellite data and radiosonde data yielded a slight moist bias against the radiosonde data (of the order of a few percent, but strongly varying between RS stations). It also yielded a significant moist bias against HIRS UTH data (7−9%RH, depending on HIRS UTH algorithm). Furthermore, it yielded a modest dry bias against AIRS V4 and V5 data (less than 3%RH). All these biases are broadly consistent with expectations based on earlier studies. UTH data standard deviations are below 3%RH against radiosonde data, approximately 6%RH against HIRS UTH data, and approximately 4%RH against AIRS UTH data.

[79] We hope that this data set will be useful for climate applications. We plan to extend the temporal coverage of the data set, by processing the older data from the SSM/T-2 instrument on DMSP F11 to F15. That data record starts in 1994, which would give us a 14-year time series of UTH.

[80] Concerning the extension of the time series into the future, one has to take into account that the AMSU-B instrument is being replaced by the MHS instrument in new satellites, starting with N18 and MetOp A. The channel characteristics of MHS are very similar to AMSU-B, but unfortunately not identical. According to *Kleespies and Watts* [2007], the brightness temperature bias between AMSU-B and MHS for Channel 18 is approximately 0.1 K, with a standard deviation of also approximately 0.1 K. (These numbers are based on radiative transfer simulations for a diverse atmospheric profile data set.) Uncorrected, this would introduce approximately 1% relative bias into the UTH data, as can be seen from equation (1). While this is small, it would still be better not to use the scaling coefficients for AMSU-B, but do the regression again to derive new coefficients for MHS. With dedicated scaling coefficients, the bias between AMSU-B and MHS for the UTH data should be very small, if both instruments were perfectly calibrated. Future studies will document the actual bias between the data sets.

References

Allan, R. P., M. A. Ringer, and A. Slingo (2003), Evaluation of moisture in the Hadley centre climate model using simulations of HIRS water-vapour channel radiances, *Q. J. R. Meteorol. Soc.*, *129*, 3371–3389, doi:10.1256/qj.02.217.

Atkinson, N. C. (2001), Calibration, monitoring and validation of AMSU-B, *Adv. Space. Res.*, *28*(1), 117–126.

Atkinson, N. C., and K. W. Whyte (2003), Further development of the ATOVS and AVHRR processing package (AAPP), including an initial assessment of EARS radiances, in *Proceedings of the Thirteenth International TOVS Study Conference*, edited by R. Saunders and T. Achtor, pp. 444–451, Int. ATOVS Working Group, Sainte-Adele, Quebec, Canada.

Aumann, H. H., et al. (2003), AIRS/AMSU/HSB on the aqua mission: Design, science objectives, data products, and processing systems, *IEEE T. Geosci. Remote*, *41*(2), 253–264.

Bates, J. J., and D. L. Jackson (2001), Trends in upper-tropospheric humidity, *Geophys. Res. Lett.*, *28*(9), 1695–1698.

Bates, J. J., D. L. Jackson, F.-B. Breon, and Z. D. Bergen (2001), Variability of tropical upper tropospheric humidity 1979–1998, *J. Geophys. Res.*, *106*(D23), 32,271–32,281.

Berg, W., J. J. Bates, and D. L. Jackson (1999), Analysis of upper-tropospheric water vapor brightness temperatures from SSM/T2, HIRS, and GMS-5 VISSR, *J. Appl. Meteorol.*, *38*, 580–595.

Buehler, S. A., and V. O. John (2005), A simple method to relate microwave radiances to upper tropospheric humidity, *J. Geophys. Res.*, *110*, D02110, doi:10.1029/2004JD005111.

Buehler, S. A., M. Kuvatov, V. O. John, U. Leiterer, and H. Dier (2004), Comparison of microwave satellite humidity data and radiosonde profiles: A case study, *J. Geophys. Res.*, *109*, D13103, doi:10.1029/2004JD004605.

Buehler, S. A., P. Eriksson, T. Kuhn, A. von Engeln, and C. Verdes (2005a), ARTS, the atmospheric radiative transfer simulator, *J. Quant. Spectrosc. Radiat. Transfer*, *91*(1), 65–93, doi:10.1016/j.jqsrt.2004.05.051.

Buehler, S. A., M. Kuvatov, and V. O. John (2005b), Scan asymmetries in AMSU-B data, *Geophys. Res. Lett.*, *32*, L24810, doi:10.1029/2005GL024747.

Buehler, S. A., M. Kuvatov, T. R. Sreerekha, V. O. John, B. Rydberg, P. Eriksson, and J. Notholt (2007), A cloud filtering method for microwave upper tropospheric humidity measurements, *Atmos. Chem. Phys.*, *7*(21), 5531–5542.

Chen, M., R. B. Rood, and W. G. Read (1999), Seasonal variations of upper tropospheric water vapor and high clouds observed from satellites, *J. Geophys. Res.*, *104*(D6), 6193–6198.

Chung, E. S., B. J. Sohn, and V. Ramanathan (2004), Moistening processes in the upper troposphere by deep convection: A case study over the tropical Indian Ocean, *J. Meteorol. Soc. Jpn.*, *82*(3), 959–965.

Chung, E. S., B. J. Sohn, J. Schmetz, and M. Koenig (2007), Diurnal variation of upper tropospheric humidity and its relations to convective activities over tropical Africa, *Atmos. Chem. Phys.*, *7*(10), 2489–2502.

Cuddy, D. T., M. D. Echeverri, P. A. Wagner, A. Hanzel, and R. A. Fuller (2006), EOS MLS science data processing system: A description of architecture and capabilities, *IEEE T. Geosci. Remote*, *44*(5), 1192–1198.

de F. Forster, P. M., and M. Collins (2004), Quantifying the water vapour feedback associated with post-Pinatubo global cooling, *Clim. Dyn.*, *23*(2), 207–214.

Elliott, W. P., R. J. Ross, and W. H. Blackmore (2002), Recent changes in NWS upper-air observations with emphasis on changes from VIZ to vaisala radiosondes, *Bull. Am. Meteorol. Soc.*, pp. 1003–1017.

Gettelman, A., W. D. Collins, E. J. Fetzer, A. Eldering, F. W. Irion, P. B. Duffy, and G. Bala (2006), Climatology of upper-tropospheric relative humidity from the atmospheric infrared sounder and implications for climate, *J. Clim.*, *19*(23), 6104–6121, doi:10.1175/JCLI3956.1.

Greenwald, T. J., and S. A. Christopher (2002), Effect of cold clouds on satellite measurements near 183 GHz, *J. Geophys. Res.*, *107*(D13), 4170, doi:10.1029/2000JD000258.

Held, I. M., and B. J. Soden (2000), Water vapor feedback and global warming, *Annu. Rev. Energy Environ.*, *25*, 441–475, doi:10.1146/annurev.energy.25.1.441.

Jackson, D. L., and J. J. Bates (2001), Upper tropospheric humidity algorithm assessment, *J. Geophys. Res.*, *106*(D23), 32,259–32,270.

Jimenez, C., P. Eriksson, V. O. John, and S. A. Buehler (2005), A practical demonstration on AMSU retrieval precision for upper tropospheric humidity by a non-linear multi-channel regression method, *Atmos. Chem. Phys.*, *5*, 451–459.

John, V. O., and S. A. Buehler (2005), Comparison of microwave satellite humidity data and radiosonde profiles: A survey of European stations, *Atmos. Chem. Phys.*, *5*, 1843–1853, sRef-ID:1680-7324/acp/2005-5-1843.

John, V. O., and B. J. Soden (2007), Temperature and humidity biases in global climate models and their impact on climate feedbacks, *Geophys. Res. Lett.*, *34*, L18704, doi:10.1029/2007GL030429.

John, V. O., S. A. Buehler, and N. Courcoux (2006), A cautionary note on the use of Gaussian statistics in satellite based UTH climatologies, *IEEE Geosci. Remote Sens. Lett.*, *3*(1), 130–134, doi:10.1109/LGRS.2005.859350.

Kahn, B. H., A. Eldering, A. J. Braverman, E. J. Fetzer, J. H. Jiang, E. Fishbein, and D. L. Wu (2007), Toward the characterization of upper tropospheric clouds using atmospheric infrared sounder and microwave limb sounder observations, *J. Geophys. Res.*, *112*, D05202, doi:10.1029/2006JD007336.

Kleespies, T. J., and P. Watts (2007), Comparison of simulated radiances, Jacobians and linear error analysis for the Microwave Humidity Sounder and the Advanced Microwave Sounding Unit-B, *Q. J. R. Meteorol. Soc.*, *132*, 3001–3010.

Lanzante, J. R., and G. E. Gahrs (2000), The "clear-sky bias" of TOVS upper-tropospheric humidity, *J. Clim.*, *13*, 4034–4041.

Lindzen, R. S., M.-D. Chou, and A. Y. Hou (2001), Does the earth have an adaptive infrared iris?, *Bull. Am. Meteorol. Soc.*, *82*(3), 417–432.

Minschwaner, K., and A. E. Dessler (2004), Water vapor feedback in the tropical upper troposphere: Model results and observations, *J. Clim.*, *17*, 1272–1282.

Read, W. G., J. W. Waters, D. A. Flower, L. Froidevaux, R. F. Jarnot, D. L. Hartmann, R. S. Harwood, and R. B. Rood (1995), Upper-tropospheric water vapor from UARS MLS, *Bull. Am. Meteorolt. Soc.*, *76*(12), 2381–2389, doi:10.1175/1520-0477(1995)076<2381: UTWVFM>2.0.CO;2.

Rosenkranz, P. W. (2001), Retrieval of temperature and moisture profiles from AMSU-A and AMSU-B measurements, *IEEE Geosci. Remote Sens.*, *39*(11), 2429–2435.

Saunders, R. W., T. J. Hewison, S. J. Stringer, and N. C. Atkinson (1995), The radiometric characterization of AMSU-B, *IEEE Trans. Microwave Theory Tech.*, *43*(4), 760–771.

Saunders, R., M. Matricardi, and P. Brunel (1999), An improved fast radiative transfer model for assimilation of satellite radiance observations, *Q. J. R. Meteorol. Soc.*, *125*, 1407–1425.

Smith, W. L., H. M. Woolf, C. M. Hayden, D. Q. Wark, and L. M. McMillin (1979), The TIROS-N operational vertical sounder, *Bull. Am. Meteorol. Soc.*, *60*, 1177–1187.

Soden, B. J., and F. P. Bretherton (1993), Upper tropospheric relative humidity from the GOES 6.7 μm channel: Method and climatology for July 1987, *J. Geophys. Res.*, *98*(D9), 16,669–16,688.

Soden, B. J., and F. P. Bretherton (1996), Interpretation of TOVS water vapor radiances in terms of layer-average relative humidities: Method and climatology for the upper, middle, and lower troposphere, *J. Geophys. Res.*, *101*(D5), 9333–9343.

Soden, B. J., and R. Fu (1995), A satellite analysis of deep convection, upper-tropospheric humidity, and the greenhouse effect, *J. Clim.*, *8*, 2333–2351.

Soden, B. J., and I. M. Held (2006), An assessment of climate feedbacks in coupled ocean-atmosphere models, *J. Clim.*, *19*(14), 3354–3360.

Soden, B. J., and J. R. Lanzante (1996), An assessment of satellite and radiosonde climatologies of upper-tropospheric water vapor, *J. Clim.*, *9*, 1235–1250.

Soden, B. J., D. D. Turner, B. M. Lesht, and L. M. Miloshevich (2004), An analysis of satellite, radiosonde, and lidar observations of upper tropospheric water vapor from the atmospheric radiation measurement program, *J. Geophys. Res.*, *109*, D04105, doi:10.1029/2003JD003828.

Soden, B. J., D. J. Jackson, V. Ramaswamy, M. D. Schwarzkopf, and X. Huang (2005), The radiative signature of upper tropospheric moistening, *Science*, *310*(5749), 841–844, doi:10.1126/science.1115602.

Spangenberg, D. A., G. G. Mace, T. P. Ackerman, N. L. Seaman, and B. J. Soden (1997), Evaluation of model-simulated upper troposphere humidity using 6.7 μm satellite observations, *J. Geophys. Res.*, *102*(D22), 25,737–25,749.

Tian, B., B. J. Soden, and X. Wu (2004), Diurnal cycle of convection, clouds, and water vapor in the tropical upper troposphere: Satellites versus a general circulation model, *J. Geophys. Res.*, *109*, D10101, doi:10.1029/2003JD004117.

Tobin, D. C., et al. (2006), Atmospheric radiation measurement site atmospheric state best estimates for atmospheric infrared sounder temperature and water vapor retrieval validation, *J. Geophys. Res.*, *111*, D09S14, doi:10.1029/2005JD006103.

Trenberth, K. E., J. Fasullo, and L. Smith (2005), Trends and variability in column-integrated atmospheric water vapor, *Clim. Dyn.*, *24*, 741–758.

Turner, D. D., B. M. Lesht, S. A. Clough, J. C. Liljegren, H. E. Revercomb, and D. C. Tobin (2003), Dry bias and variability in vaisala RS80-H radiosondes: The ARM experience, *J. Atmos. Ocean Technol.*, *20*, 117–132.

————————————

S. Buehler and M. Milz, Institutionen för Rymdvetenskap (Department of Space Science) (IRV), Luleå University of Technology, Box 812, Kiruna 98128, Sweden. (sbuehler@ltu.se)

D. L. Jackson, Cooperative Institute for Research in Environmental Science (CIRES), University of Colorado/NOAA Earth System Research Laboratory, 325 Broadway R/PSD2, Boulder, CO 80305-3337, USA.

V. O. John, Met Office Hadley Centre, FitzRoy Road, Exeter, EX1 3PB, UK.

M. Kuvatov, German Weather Service (Deutscher Wetterdienst, DWD), Frankfurterstr. 135, 63067 Offenbach am Main, Germany.

J. Notholt, Institut für Umweltphysik (Institute for Environmental Physics) (IUP), University of Bremen, Bremen, Germany.

B. J. Soden, Rosenstiel School for Marine and Atmospheric Science (RSMAS), University of Miami, 4600 Rickenbacker Causeway, Miami, FL 33149, USA.